Markov chain analysis of random walks in disordered media

Sonali Mukherjee, Hisao Nakanishi, and Norman H. Fuchs
Department of Physics, Purdue University, West Lafayette, Indiana 47907
(Received 4 November 1993; revised manuscript received 2 February 1994)

We study the dynamical exponents d_w and d_s for a particle diffusing in a disordered medium (modeled by a percolation cluster), from the regime of extreme disorder (i.e., when the percolation cluster is a fractal at $p = p_c$) to the Lorentz gas regime when the cluster has weak disorder at $p > p_c$ and the leading behavior is standard diffusion. The velocity autocorrelation function and the return to the starting point probability are related to the asymptotic spectral properties of the hopping transition probability matrix of the diffusing particle; the latter is numerically analyzed by the Arnoldi-Saad algorithm. We propose and present evidence for a scaling relation for the second largest eigenvalue in terms of the size of the cluster, $|\ln\lambda_2| \sim S^{-d_w/d_f}$. This relation provides a very efficient and accurate method of extracting the spectral dimension d_s where $d_s = 2d_f/d_w$.

PACS number(s): 05.40.+j, 05.50.+q, 64.60.Fr

I. INTRODUCTION

Random walks have held the interest of physicists, engineers, and mathematicians for a long time now, partly due to their ability to model a wide variety of problems which can be described at some level by transitions in states which are governed by probabilistic laws. For example, random walks have been used extensively to model the motion of a particle in diffusive processes through solids (ordered or disordered), liquid, or gas, including transport problems like electrical conduction [1,2], and in describing certain conformational properties of macromolecules [3,4].

In this paper we present an approach to studying random walks which is an alternative to the more common one where the individual random walk is pursued either by simulation or in some other way. This is the method of spectral analysis of the corresponding transition probability matrix. This method allows us to relate the various dynamical quantities of the walk, such as the velocity autocorrelation function, $\langle \mathbf{v}(t) \cdot \mathbf{v}(0) \rangle$, the return to the starting point probability after t steps, $P(t)$, the mean square displacement, and the acceleration autocorrelation function, to the asymptotic spectral properties of the transition probability matrix $\mathbf{W}$ (defined below). With the development of the various numerical methods of diagonalizing large matrices, this approach can serve as a very powerful tool to solve for these dynamical quantities.

In this work, we model a random medium by a percolation cluster, where sites on a lattice are occupied with probability p (otherwise empty) and the occupied nearest neighbor sites are considered to be connected [5]. It is well known that there is a critical threshold p_c where the *incipient* infinite cluster is a disordered fractal [6]. Such a cluster will serve as an example of a random medium with a critically correlated disorder. We will also confine our attention for the moment to the random walk which takes place on the (critical or noncritical) percolation cluster according to the so-called blind or myopic ant rule. The blind ant moves to an occupied nearest neighbor in one time step with equal probability of $1/z$ (where z is the coordination number of the underlying lattice) and it remains at the same site with the probability equal to $(z - z_i)/z$ (where z_i is the number of occupied nearest neighbors of that particular site), thus yielding some dispersion in the waiting time before a hopping event takes place. On the other hand, the myopic ant never stays at the same site but always moves to an occupied nearest neighbor with equal probability $1/z_i$ at each time step [7]. For our purposes, the blind and myopic ants simply represent the simplest rules to yield Brownian dynamics. However, they could be argued to reflect the appropriate features of some specific diffusion phenomena: e.g., the dispersion in waiting times for the blind ant might make it more suitable to mimic hopping electrical conduction in disordered semiconductors while a myopic ant might be preferred to mimic fluid flow through a porous medium.

The transition probability matrix $\mathbf{W}$ is defined as the matrix with its ijth element equal to the probability that a particle at site j hops to site i in the next time step. Both the blind and myopic ants can be described by a matrix $\mathbf{W}$ which is a Markov matrix [8] as each element is equal to or greater than zero and the sum of all the elements of each column is equal to 1. Such a matrix describes a *Markov chain*, which is a one-dimensional, discrete Markov process.

In this paper we will mainly concentrate on the two important quantities for the random walker, $\langle \mathbf{v}(t) \cdot \mathbf{v}(0) \rangle$ and $P(t)$. At $p = p_c$ blind and myopic ants are known to exhibit a nondiffusive leading behavior called *anomalous* diffusion [9]. In this case, the walk is often characterized by a *walk dimension* d_w where its mean square displacement after t steps $\langle \mathbf{R}(t)^2 \rangle$ is given by

$$\langle \mathbf{R}(t)^2 \rangle \sim t^{2/d_w}. \tag{1}$$

The deviation of d_w from 2 is a measure of the nonstandard nature of the random walk.

In a stationary ensemble (that is, where the correlation functions depend only on the relative time difference and not on the absolute times), the second derivative of $\langle \mathbf{R}(t)^2 \rangle$ is proportional to $\langle \mathbf{v}(t) \cdot \mathbf{v}(0) \rangle$. So under these conditions $\langle \mathbf{v}(t) \cdot \mathbf{v}(0) \rangle$ is normally expected to obey the following power law in the long-time limit:

$$\langle \mathbf{v}(t) \cdot \mathbf{v}(0) \rangle \sim t^{2/d_w - 2}. \tag{2}$$

Such a behavior is common for the blind ant and also for the myopic ant on so-called nonbipartite lattices at least asymptotically [although the leading behavior in the velocity autocorrelation for the myopic ant on bipartite lattices does not derive from that of $\langle R(t)^2 \rangle$, thus providing exceptions to this behavior]. A lattice (or a cluster) is called bipartite if it can be partitioned into two equivalent classes of sites where all connectivity is between sites of different classes.

The long-time behavior of the probability $P(t)$ that a random walker returns to the starting point at time t is also generally a power law, where

$$P(t) \sim t^{-d_s/2}, \tag{3}$$

and d_s is the spectral dimension. For a standard diffusive behavior, d_s is equal to the spatial dimensionality d, while on a fractal, it is generally a fractional number different from d. Thus one can see that the two exponents d_w and d_s characterize the important quantities $\langle \mathbf{v}(t) \cdot \mathbf{v}(0) \rangle$ and $P(t)$ for the diffusion process in a fractal medium.

As p is increased above p_c, the percolation cluster becomes nonfractal, and the particle on it starts to diffuse normally at large length scales. In this case, we have a random walk with fixed scatterers placed with weakly correlated disorder, and thus we may describe this regime as the Lorentz gas regime [10,11]. In a Lorentz gas, $\langle \mathbf{v}(t) \cdot \mathbf{v}(0) \rangle$ generally exhibits a *long-time tail*, obeying the following power law:

$$\langle \mathbf{v}(t) \cdot \mathbf{v}(0) \rangle \sim t^{-d/2-1}, \tag{4}$$

and $P(t)$ scales as in normal diffusion,

$$P(t) \sim t^{-d/2}, \tag{5}$$

where d is the Euclidean dimension of the cluster.

Previously diffusion in the two regimes (the anomalous diffusion regime and the Lorentz gas regime) was often studied by using very different techniques. We show in this paper that the method of spectral analysis of the hopping transition probability matrix provides an elegant way of studying both regimes using the same method.

This work is organized as follows. In Sec. II, we review and summarize important properties of the matrix $\mathbf{W}$, and in Sec. III we discuss the significance of the eigenspectrum of $\mathbf{W}$. The particular significance of the subdominant eigenvalue λ_2 is shown in Sec. IV. In Sec. V, the Arnoldi-Saad approximate diagonalization scheme is discussed, and the main numerical results of this work are given in Sec. VI. A summary of our findings is presented in Sec. VII. A preliminary account of this work was given [12] where some of the present results were also reported. In this paper, we give new results, particularly on the scaling of the subdominant eigenvalue, as well as expanding on the results only briefly reported in the earlier work by exploring the effects of ant type, lattice, boundary conditions, and the finite size of the cluster.

II. HOPPING TRANSITION PROBABILITY MATRIX

Since the transition probability matrix $\mathbf{W}$ contains all the information about the geometry of the underlying substrate on which the random walk takes place and also the kinematics of the walk itself, all the characteristics of the walk can be extracted from this matrix. Because of the importance of $\mathbf{W}$ we enumerate in this section some properties of $\mathbf{W}$, especially of its eigenvalue spectrum. Much of the information is hidden in its eigenvalue spectrum as will be elucidated later. Some of the properties discussed here are already well known but are reproduced here for completeness, while others are not commonly appreciated despite their potential usefulness.

A. Basic properties

By definition, Markov matrices must have the following two properties. First, for all i and j,

$$W_{ij} \geq 0, \tag{6}$$

and second

$$\sum_i W_{ij} = 1. \tag{7}$$

The second property ensures the presence of the eigenvalue 1 with at least one normalized left eigenvector having all components positive and of the same magnitude. There is also a corresponding normalized right eigenvector with eigenvalue 1. This right eigenvector in fact represents the equilibrium probability distribution of the diffusing particle. Thus, for a connected cluster (with no isolated, unreacheable part), the corresponding eigenvector of $\mathbf{W}$ can be made positive definite.

It is well known that the eigenvalues of the Markov matrix satisfy

$$|\lambda| \leq 1. \tag{8}$$

For completeness' sake a proof is given in Appendix A.

B. Detailed and extended detailed balance

The transition matrix $\mathbf{W}$ is said to satisfy the detailed balance condition if its elements satisfy the following condition for all (i,j):

$$W_{ij}\rho_j^e = W_{ji}\rho_i^e, \tag{9}$$

where ρ_j^e is the jth element of the equilibrium proba-

bility distribution, i.e., the normalized, positive-definite right eigenvector of **W** for the eigenvalue 1. It is easy to show that **W** satisfying the detailed balance condition can be transformed into a symmetric matrix by a similarity transformation, thus proving that all eigenvalues of **W** are real. The proof is given in Appendix B.

The matrix **W** is said to satisfy the extended detailed balance condition of order n if it sastisfies the following property for all (i,j):

$$(W^p)_{ij}\rho_j^e = (W^p)_{ji}\rho_i^e \tag{10}$$

for $p = n$ but not for $p = n-1$. From the previous argument on the detailed balance condition we can say that all eigenvalues of $\mathbf{W}^n$ are real if **W** satisfies this condition. But **W** will in general have complex eigenvalues in conjugate pairs (as **W** itself is real). Thus all complex eigenvalues of **W** are such that λ^n are real, as the eigenvalues of $\mathbf{W}^n$ are just the nth power of those of **W**. Therefore, all the complex eigenvalues of **W** which have the same magnitude converge to either a single real eigenvalue for $\mathbf{W}^n$ (which is λ^n) or to the two values $\pm|\lambda^n|$. Since the eigenvectors of **W** and $\mathbf{W}^n$ are the same, all the linearly independent eigenvectors corresponding to the different eigenvalues having the same magnitude will have the same one or two eigenvalues, producing a degeneracy of order at most n for $\mathbf{W}^n$.

The detailed balance condition is satisfied by most models of diffusion (such as the blind and myopic ant random walks considered here), but it is possible to violate it by considering, e.g., *directed* walks. A particularly simple example is a random walk taking place on a unit square but with a preference for moving clockwise. In this case, the detailed balance is not obeyed, but the extended detailed balance *is* obeyed at the fourth order. More involved examples may be found when the kinetic rules of diffusion induce the formation of *vortices*, reminiscent of what actually happens in turbulence.

C. Oscillations in autocorrelations

The position autocorrelation function can be expanded in terms of the real (positive and negative) and complex eigenvalues in the following way:

$$\langle \mathbf{r}(n)\cdot\mathbf{r}(0)\rangle = \sum_{\lambda_+} a(\lambda_+)\lambda_+^n + (-1)^n \sum_{\lambda_-} a(\lambda_-)\lambda_-^n + \sum_{\lambda_c,\omega} 2a(\lambda_c,\omega)\cos[\omega n + \phi(\lambda_c,\omega)]\lambda_c^n, \tag{11}$$

where λ_+ and $-\lambda_-$ are real, positive and negative eigenvalues, respectively, and $\lambda_c e^{i\omega}$ denotes a complex eigenvalue with modulus λ_c. The last sum is over the complex eigenvalues and thus relevant only for the matrices **W** which do not satisfy the detailed balance condition. The cosine term arises in this case because the complex roots come in conjugate pairs. This term, if present, gives rise to oscillations in the position autocorrelation function, different from the even-odd oscillation that stems from the negative real eigenvalues. This oscillation is persistent (shows up even in the long-time limit) if the term λ_c^n is equal to 1. For $\lambda < 1$, the oscillation is exponentially damped.

Thus **W** (if it does not satisfy the detailed balance condition) can have both persistent and transient oscillations in the position autocorrelation function of period larger than 2. Now, if **W** satisfies the extended detailed balance of order n, then the autocorrelations will have oscillations of period at most $2n$, again either persistent or transient depending on the modulus of the eigenvalue causing the oscillation. In this way, the order of the extended detailed balance and the period of oscillation in the autocorrelation are closely related. This is intuitively acceptable when we consider the case of vortices for a typical example of **W** satisfying the extended detailed balance condition.

D. Myopic and blind ant

In light of the above discussion, let us now concentrate on the properties of **W** for the myopic and blind ants specifically. A blind ant in a disordered medium has a symmetric **W** as all the nonzero off-diagonal elements are equal to the same value $1/z$ (where z is the coordination number of the lattice). Thus all its eigenvalues are real. It does not has an eigenvalue equal to -1, so its position autocorrelation function can only have transient, even-odd oscillation.

On the other hand, **W** for the myopic ant is not symmetric as the hopping probability depends on the location of the random walker, that is, it is equal to $1/z_i$, where z_i is the number of occupied nearest neighbors of the particular site. However, it does satisfy the detailed balance condition, and thus can be transformed into a symmetric matrix by a similarity transformation as seen before. Thus the myopic ant also can have at most an even-odd oscillation. However, such an oscillation can be persistent since an eigenvalue -1 is possible. This occurs when the cluster is bipartite. This is because the myopic ant on a bipartite cluster has eigenvalues in pairs of λ and $-\lambda$, as can be seen easily by converting an eigenvector corresponding to eigenvalue λ into one corresponding to eigenvalue $-\lambda$ by simply making the components corresponding to the sites of one of the subclusters opposite in sign. Myopic ants on a nonbipartite cluster, however, can only have a transient, even-odd oscillation.

III. EIGENSPECTRUM OF W AND DYNAMICS OF THE WALK

Now we embark on the task of understanding the eigenspectrum of **W** and building up the connection between the spectrum and the characteristic functions of the walk in the time domain (such as the velocity autocorrelation function and the return to the starting point probability).

A. Density of eigenvalues $n(\lambda)$

In this work, let us define the density of eigenvalues $n(\lambda)$ as the number of eigenvalues of $\mathbf{W}$ normalized by the range of λ as well as by the number of sites S in the cluster. (This differs from the convention used in [12] by a factor of S.) The densities $n(\lambda)$ for the blind and myopic ants show some interesting common characteristics. First, at the critical dilution $p = p_c$, the eigenvalues accumulate as $\lambda \to 1$, which results in a power law increase of $n(\lambda)$ as $\ln\lambda \to 0$. As p is increased from its critical value, the piling up of the eigenvalues diminishes and the value of $n(\lambda)$ averaged over small regions of λ either flattens (in $d = 2$) or actually decreases (in $d = 3$) as $\ln\lambda \to 0$. This is illustrated in Fig. 1 where $n(\lambda)$ for the myopic ant on a small square lattice is plotted for $p = 0.593 \approx p_c$ and $p = 0.8 > p_c$. Second, the eigenvalue spectrum shows sharp peaks at certain characteristic values of λ in a region far from the asymptotic limit of $\lambda \to 1$. This is better illustrated in Fig. 2 for the blind ant on a small lattice. These observations are discussed in more detail below.

First, we recall the connection between the density $n(\lambda)$ and the probability $P(t)$ that the diffusing particle returns to the starting point at time t. The mean probability $P(t)$ can be expressed in terms of the corresponding probability $P_i(t)$ for a given starting point i as

$$P(t) = \sum_i P_i(t)\rho_0(i), \tag{12}$$

where $\rho_0(i)$ is the probability for the particle to be at site i initially. When the initial distribution is the equilibrium one (as we normally assume), this probability is uniformly equal to $1/S$ (where S is the cluster size) for the blind ant while, for the myopic ant, it fluctuates from site to site according to the local coordination number. In either case, $P_i(t)$ is given by

$$P_i(t) = \mathbf{e}_i^T \mathbf{W}^t \mathbf{e}_i, \tag{13}$$

where $\mathbf{e}_i$ is the column vector whose components are all zeros except the ith component which is 1 and $\mathbf{e}_i^T$ is the corresponding row vector of $\mathbf{e}_i$. The superscript T refers to the *transpose* in the matrix notation.

Below we assume the blind ant for simplicity, but the final result is essentially the same for the myopic ant as will be noted. Thus,

$$P(t) = \mathrm{Tr}\mathbf{W}^t/S = \sum_i {\lambda_i}^t/S. \tag{14}$$

Since -1 is not an eigenvalue for the blind ant and there is a buildup of eigenvalues only near $\lambda = 1$ (for $p = p_c$), and since we are only interested in the long-time limit where the dominant contribution comes from the eigenvalues near 1, we can neglect the contribution of the negative eigenvalues. Thus summing the eigenvalues in the above equation only over $\lambda > 0$ and by taking the inverse Laplace transform, we get

$$\begin{aligned}\frac{1}{2\pi i}\int_\Gamma e^{Ez}\mathrm{Tr}\mathbf{W}^z/S &\approx \sum_{\lambda>0}\frac{1}{2\pi}\int_{-\infty}^{\infty} dt e^{i(E-|\ln\lambda|)t}/S \\ &= \sum_{\lambda>0}\delta(E-|\ln\lambda|)/S,\end{aligned} \tag{15}$$

where Eq. (14) has been continued analytically to the complex plane and Γ is along the imaginary axis.

The quantity on the right is the density of eigenvalues as normalized in E (i.e., in the space of $\ln\lambda$), but for small E (or for eigenvalues near 1), it reduces to $n(\lambda)$.

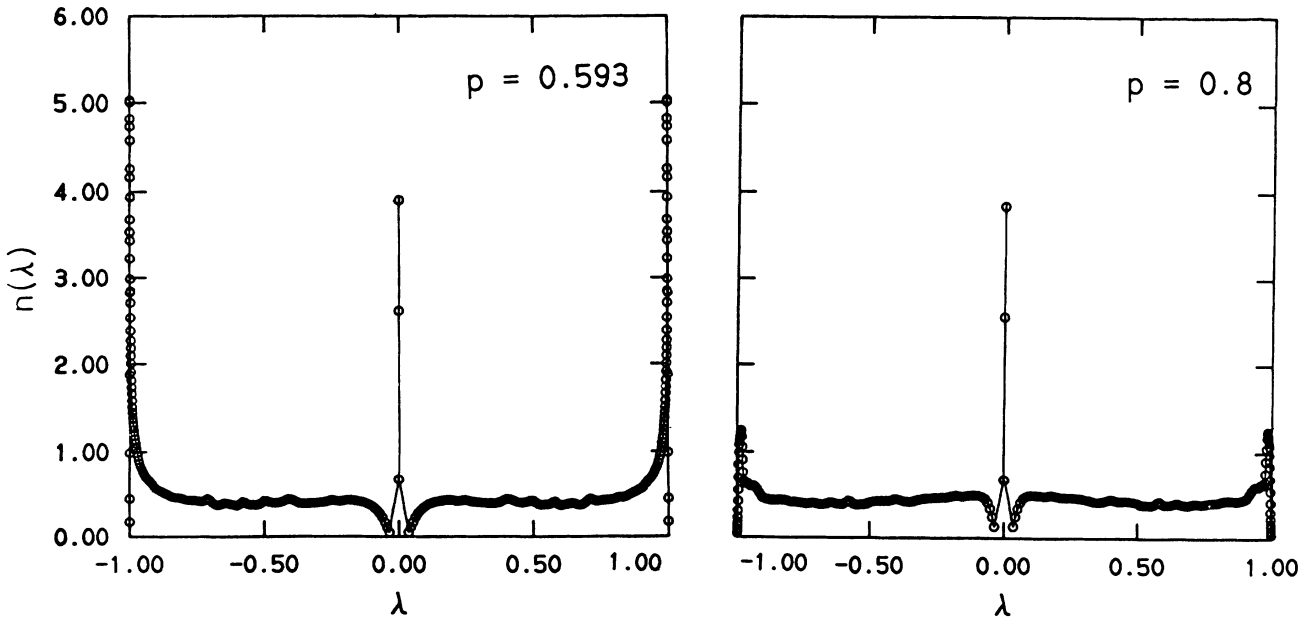

FIG. 1. Density of eigenvalues $n(\lambda)$ for the myopic ant on the square lattice cluster of size 200 at $p = 0.593 \approx p_c$ and $p = 0.8$. This figure shows the buildup of $n(\lambda)$ near $\lambda = \pm 1$ at $p = 0.593$ and the flattening of $n(\lambda)$ for $p > p_c$.

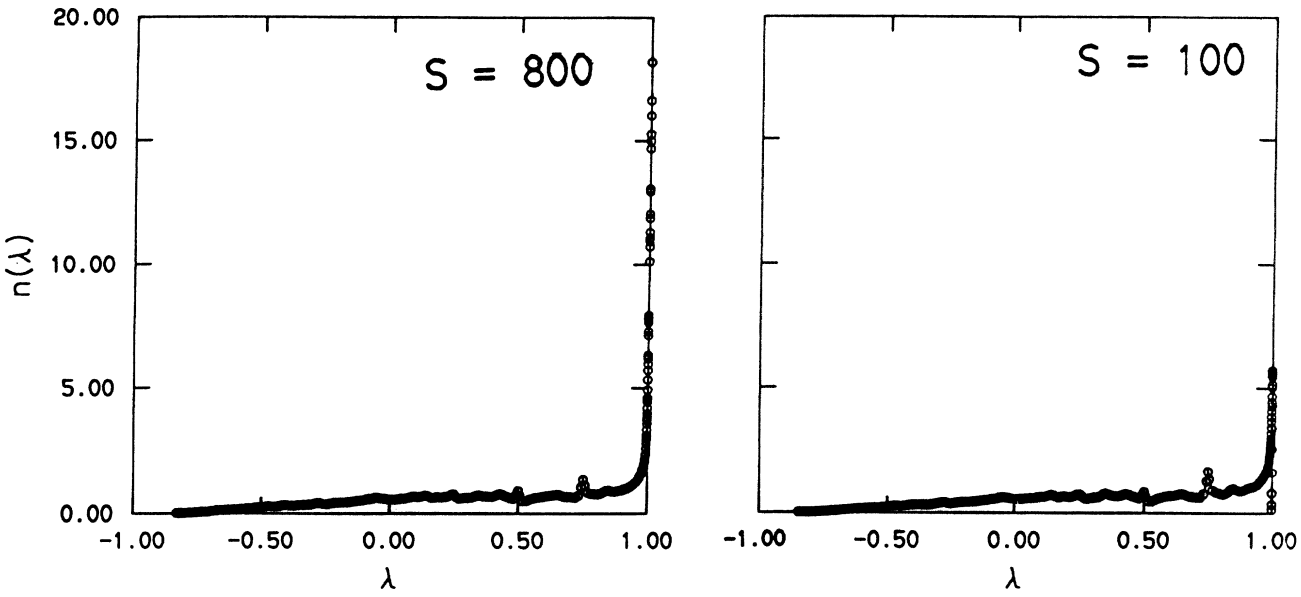

FIG. 2. Density of eigenvalues $n(\lambda)$ at $p = 0.593$ for the blind ant on small square lattice clusters of size 800 and 100 sites. This figure shows the peaks due to the local structures of the cluster as well as the increase in $n(\lambda)$ near 1 for larger size clusters.

Thus we see that $P(t)$ is the Laplace transform of the (normalized) $n(\lambda)$, at least for large t where the neglect of $\lambda < 0$ is unimportant. Although the above discussion has been for the blind ant, the calculation for the myopic ant is also very similar. In the latter case, $P(t)$ will be bounded by the Laplace transform of $n(\lambda)$ multiplied by two different coefficients.

Since $P(t)$ for the ants in general decays for large t following a power law [7]

$$P(t) \sim t^{-d_s/2}, \tag{16}$$

the Laplace relationship implies for both blind and myopic ants

$$n(\lambda) \sim |\ln \lambda|^{d_s/2-1}. \tag{17}$$

Similarly for $p > p_c$, $P(t)$ decays as

$$P(t) \sim t^{-d/2}, \tag{18}$$

where d is the Euclidean dimension of the lattice, leading to

$$n(\lambda) \sim |\ln \lambda|^{d/2-1}. \tag{19}$$

B. Autocorrelation function

The position autocorrelation function of a diffusing particle can be expressed in the following way:

$$\langle \mathbf{r}(t) \cdot \mathbf{r}(0) \rangle = \mathbf{X}^T \mathbf{W}^t \mathbf{X_o} + \mathbf{Y}^T \mathbf{W}^t \mathbf{Y_o} + \mathbf{Z}^T \mathbf{W}^t \mathbf{Z_o}, \tag{20}$$

where $\mathbf{X}^T$, $\mathbf{Y}^T$, and $\mathbf{Z}^T$ are the row vectors whose components are the x, y, and z components of the corresponding sites, respectively, while $\mathbf{X_o}$, $\mathbf{Y_o}$, and $\mathbf{Z_o}$ are the column vectors whose ith components are equal to $\rho_i X_i$, $\rho_i Y_i$, and $\rho_i Z_i$, respectively, where ρ is the initial probability distribution for the random walker.

The vectors $\mathbf{X}^T$, $\mathbf{Y}^T$, and $\mathbf{Z}^T$ can be expanded in terms of the eigenvectors of the transition matrix $\mathbf{W}$. For example, we have

$$\mathbf{X}^T = \sum_\lambda b_\lambda^x \mathbf{u}_\lambda^T, \tag{21}$$

where b_λ^x is the expansion coefficient and $\mathbf{u}_\lambda^T$ is the normalized left eigenvector with the eigenvalue λ. Similarly the vectors $\mathbf{X_o}$, $\mathbf{Y_o}$, and $\mathbf{Z_o}$ can be expressed in terms of the right eigenvectors of $\mathbf{W}$. For example, we can write

$$\mathbf{X_o} = \sum_\lambda c_\lambda^x \mathbf{v}_\lambda, \tag{22}$$

where $\mathbf{v}_\lambda$ is the right eigenvector with the eigenvalue λ (normalized so that $\mathbf{u}_\lambda^T \mathbf{v}_\lambda = 1$) and c_λ^x is the expansion coefficient.

Thus Eq. (20) can be expressed as

$$\langle \mathbf{r}(t) \cdot \mathbf{r}(0) \rangle = \sum_\lambda (b_\lambda^x c_\lambda^x + b_\lambda^y c_\lambda^y + b_\lambda^z c_\lambda^z) \lambda^t, \tag{23}$$

noting that the normalized eigenvectors $\mathbf{u}_\lambda^T$ and $\mathbf{v}_{\lambda'}$ are orthogonal to each other if the eigenvalues λ, λ' are different. Further denoting

$$a_\lambda \equiv \vec{b}_\lambda \cdot \vec{c}_\lambda, \tag{24}$$

where the vector sign and dot product refer to the coordinate space, we can write

$$\langle \mathbf{r}(t) \cdot \mathbf{r}(0) \rangle = \sum_\lambda a_\lambda \lambda^t. \tag{25}$$

The coefficients a_λ can be calculated either directly from Eq. (24) or, as we did in the case of the periodic boundary condition, from a modified form as given in Appendix C.

Though we have calculated the position autocorrelation function here, other correlation and autocorrelation functions can also be calculated in a similar way. This includes the mean square displacement $\langle[\mathbf{r}(t)-\mathbf{r}(0)]^2\rangle$ and position-velocity cross correlation $\langle\mathbf{r}(t)\cdot\mathbf{v}(t)\rangle$, as well as the velocity autocorrelation function. The latter has been shown [13] to be related to the eigenspectrum of $\mathbf{W}$ in the following way:

$$\langle\mathbf{v}(t)\cdot\mathbf{v}(0)\rangle = -\sum_\lambda a_\lambda(\lambda-1)^2\lambda^t. \tag{26}$$

Since the eigenspectrum of the myopic ant on a bipartite cluster contains both the eigenvalues 1 and -1, after *all* the transients have died out, its position autocorrelation function behaves as

$$\langle\mathbf{r}(t)\cdot\mathbf{r}(0)\rangle \sim a_1 + a_{-1}(-1)^n. \tag{27}$$

That is, the position autocorrelation has an undamped oscillation about the value a_1. If the cluster is nonbipartite or if the ant is a blind ant, then there is no eigenvalue -1, and thus there will be no undamped oscillations. It can easily be seen from Eq. (26) that the corresponding velocity autocorrelation for the myopic ant on a bipartite cluster also has an undamped oscillation. However, because of the factor $(\lambda-1)^2$, this persistent oscillation is symmetric about zero as shown in [14]. Again, if the cluster is not bipartite or if the ant is a blind ant, then such an undamped oscillation will not exist.

Since the long-time behavior of autocorrelations for the blind ant and the myopic ant on a nonbipartite cluster are (normally) dominated by the eigenspectrum near 1, the summation over the eigenvalues in Eq. (26) can be restricted to only the positive ones. For the myopic ant on a bipartite cluster, however, there is an accumulation of eigenvalues symmetrically about $\lambda=\pm1$. Thus, in this case, the factor $(\lambda-1)^2$ actually makes the eigenvalues near -1 dominate over those near 1, and the summation can be replaced by the one over only the negative eigenvalues.

Therefore, in the long-time limit, the velocity autocorrelation can be written as

$$\langle\mathbf{v}(t)\cdot\mathbf{v}(0)\rangle = -\sum_{\lambda\in\Lambda} a_\lambda(\lambda-1)^2\lambda^t, \tag{28}$$

where Λ is the set of positive eigenvalues near 1 for the blind ant and the myopic ant on a nonbipartite cluster (case A) and the set of negative eigenvalues near -1 for the myopic ant on a bipartite cluster (case B). Converting the summation in the above equation into an integral,

$$\langle\mathbf{v}(t)\cdot\mathbf{v}(0)\rangle \approx -\int_\Lambda d\lambda\pi(\lambda)\lambda^t, \tag{29}$$

where $\pi(\lambda)$ is

$$\pi(\lambda) = n(\lambda)a_\lambda S(\lambda-1)^2, \tag{30}$$

where $n(\lambda)$ is the density of eigenvalues per cluster site.

This equation can be further cast in the form of the Laplace transform in the long-time limit,

$$|\langle\mathbf{v}(t)\cdot\mathbf{v}(0)\rangle| \approx \int_0^\infty du e^{-ut}\pi(\lambda), \tag{31}$$

where $u=|\ln\lambda|$ for case A (blind ant in general and myopic ant on nonbipartite cluster), and $u=|\ln|\lambda||$ for case B (myopic ant on a bipartite cluster). This establishes the Laplace relationship between $\pi(\lambda)$ and the velocity autocorrelation. Therefore the power law behavior of the velocity autocorrelation,

$$|\langle\mathbf{v}(t)\cdot\mathbf{v}(0)\rangle| \sim t^{-y}, \tag{32}$$

implies a corresponding power law behavior in $\pi(\lambda)$,

$$\pi(\lambda) \sim u^{y-1}, \tag{33}$$

with u identified appropriately as above. Thus, by measuring the exponent $y-1$ for the function $\pi(\lambda)$, we can deduce the corresponding asymptotic behavior of the velocity autocorrelation function.

The exponent y appearing in the velocity autocorrelation depends on the two cases [12,13],

$$y = \begin{cases} 2-2/d_w & (\text{case A, at } p_c), \\ d_s/2 & (\text{case B, at } p_c), \end{cases} \tag{34}$$

for $p=p_c$, and

$$y = \begin{cases} d/2+1 & (\text{case A, } p>p_c), \\ d/2 & (\text{case B, } p>p_c), \end{cases} \tag{35}$$

for $p>p_c$. In case A, this exponent characterizes the decay of the autocorrelation which is always negative for long times (cage effect), while in case B, it describes the decrease in the envelope amplitude of the even-odd oscillation of the autocorrelation function.

In the latter case, however, the mean of the autocorrelation function from the two consecutive even-odd steps (rather than the envelope) does have the same decay behavior as in the first case. Thus, the behavior of the center line for the oscillating velocity autocorrelation for the myopic ant on bipartite clusters can be obtained from the eigenspectrum near 1, allowing it to be included with case A. In fact, some of the numerical results we present later demonstrate that such behavior leads to exactly the same exponent y as in case A.

C. Local structure in the eigenvalue spectrum

The eigenspectrum shows sharp peaks at certain characteristic values of λ. The λ at which these peaks occur depends upon the type of lattice and the kind of ant, indicating that the peaks are structures corresponding to small length scales. For example, the blind ant on the square lattice shows strong characteristic peaks at $\lambda=0.5$ and 0.75.

The presence of high degeneracies for these eigenvalues can be explained by looking at their corresponding eigen-

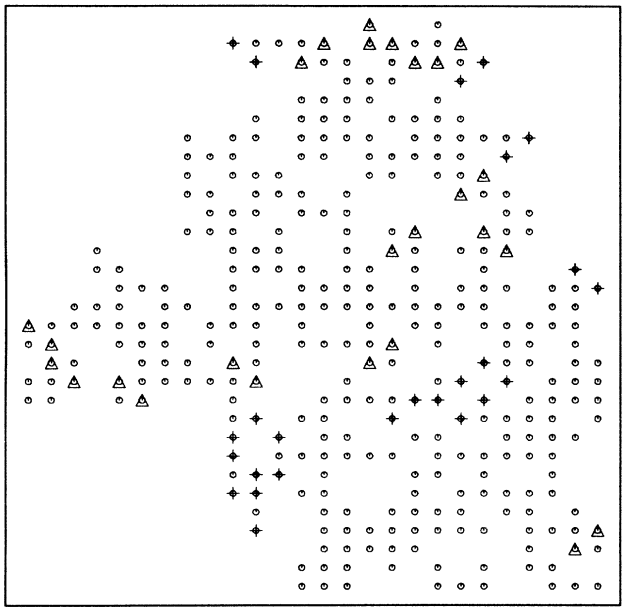

FIG. 3. Illustration of the eigenvectors which contribute to the peaks in the eigenvalue spectrum at $p = 0.75$ and $p = 0.5$ using a small cluster on the square lattice (sites shown with dots). Some (not all) such eigenvectors are chosen and the sites of nonzero amplitudes for eigenvectors with eigenvalue $\lambda = 0.75$ are marked by the symbol + and those with $\lambda = 0.5$ are marked by $\triangle$.

vectors. For example, the eigenvectors for the eigenvalue 0.5 reveal that the components corresponding to most of the sites are zero and those with nonzero values are arranged in pairs of equal magnitudes but opposite signs. In fact, they involve the diagonal arrangement of two sites of a unit square having amplitudes of opposite signs with the remaining two sites of the square having zero amplitudes. In some cases, there are additional pairs of sites with amplitudes of opposite signs hanging off such arrangements. Similarly, when one inspects the components of the eigenvectors for the eigenvalue 0.75, they are seen to involve one, two, or three dangling ends which are connected to the main part of the cluster through the same site, which has a zero amplitude. Again, in some cases, there are additional pairs of sites with nonzero amplitudes attached to such arrangements. Some examples of these arrangements are illustrated in Fig. 3.

These local structures connecting a small number of sites are simple enough to be present in large numbers for essentially all clusters of appreciable size. Thus they give the sharp peaks seen in the eigenspectra as in Fig. 1, but do not contribute much to the long-time behaviors of diffusion on the structure.

IV. SCALING FOR THE SUBDOMINANT EIGENVALUE

As we have discussed, at $p = p_c$ the eigenvalues of $\mathbf{W}$ accumulate near 1 though the eigenvalue 1 itself remains isolated from this buildup. This behavior near the eigenvalue 1 is mirrored in the region near -1 for the myopic ant on a bipartite cluster. Thus for any finite cluster there is a sharp discontinuity from the maximum eigenvalue 1 to the subdominant eigenvalue λ_2. This gap decreases to zero as the cluster size increases to infinity.

A simple scaling argument for the cluster size dependence of λ_2 can be given as follows. In the Laplace relationship between the time domain quantities and the corresponding functions of λ, the variables t and $|\ln\lambda|$ are the conjugate variables. Thus, $|\ln\lambda|^{-1}$ corresponds to a time scale. In particular, $|\ln\lambda_2|^{-1}$ corresponds to the time scale associated with the eigenmode with the eigenvalue λ_2. In terms of the mapping between the random walk and *scalar* elasticity problems [15], the vibrational energy E of a mode corresponds to $|\ln\lambda|$; thus again $|\ln\lambda|^{-1}$ corresponds to a time scale. The maximum eigenvalue 1 then corresponds to the truly *infinite* time scale, reflecting only the persistent residual behavior after all interesting dynamical behavior has been damped out.

On the other hand, the subdominant mode reflects the longest, finite time-scale dynamical behavior. Thus, this mode should reflect the geometry and size of the whole cluster. Therefore, the time scale $|\ln\lambda_2|^{-1}$ should correspond to the time it takes for a diffusing particle to *just* sample the entire cluster of size S. The latter time scales as S^{d_w/d_f}. So we expect

$$|\ln\lambda_2| \sim S^{-d_w/d_f}, \tag{36}$$

where the exponent d_w/d_f can be replaced by $2/d_s$ for structures such as the critical percolation cluster [15]. This way of calculating d_s is very efficient since it only requires the accurate determination of one eigenvalue (the second largest one) in the entire eigenspectrum. The numerical confirmation of this power law is described in the section on the numerical results.

We now propose a more general scaling relation which includes the region near but greater than p_c as follows:

$$|\ln\lambda_2| = S^{-d_w/d_f} f((p - p_c)S^{\sigma}), \tag{37}$$

where $f(x)$ is a universal scaling function and the exponent $\sigma = 1/(d_f\nu)$ is the one appearing in the usual percolation cluster size scaling [5].

In order to satisfy the known asympototic behavior for $p > p_c$, we assume that $f(x)$ satisfies the following limiting behavior:

$$f(x) = \begin{cases} \text{const}, & x \to 0, \\ x^z, & x \to \infty. \end{cases} \tag{38}$$

We see that in the $x \to 0$ limit we regain the previous relation, and the exponent z can be determined by demanding that the $x \to \infty$ limit leads to the normal diffusive behavior where $d_w = 2$ and $d_f = d$, the Euclidean dimension. Thus, in this limit we expect

$$|\ln\lambda_2| \sim S^{-2/d}. \tag{39}$$

For this to be true, we must then have

$$z = (d_w/d_f - 2/d)/\sigma. \tag{40}$$

Since the cluster is *ordered* for $p > p_c$, the scalar elasticity analog would be the phonon problem. In this case the energy of the phonons $E \sim k^2 \sim l^{-2}$, where l is a length scale of the phonon, and since the cluster has the dimensionality d, $l_{\max} \sim S^{1/d}$. Thus, we again see that $E_{\min} \sim |\ln \lambda_2| \sim S^{-2/d}$ as above. Numerical results supporting the above finite size scaling relation for $|\ln \lambda_2|$ are also given in the section on numerical results.

V. ARNOLDI-SAAD APPROXIMATE DIAGONALIZATION METHOD

In this work we have used the Arnoldi-Saad algorithm [16] in order to approximately diagonalize the transition probability matrix $\mathbf{W}$. The main advantage of using this algorithm in diagonalizing a matrix is that it allows the very accurate determination of a subset of the eigenvalues near the maximum in the spectrum. This is convenient since we are interested in the asymptotic long-time behavior of the diffusion process, which is determined by the eigenvalues near the maximum. In particular, we are mainly interested in the asymptotic power law behavior of the density of eigenvalues $n(\lambda)$ and the function $\pi(\lambda)$ as well as that of the subdominant eigenvalue λ_2 as discussed above. Both because the thermodynamic limit requires a large system and because the eigenvalues approach 1 more closely for larger size of the cluster, the accurate determination of the asymptotic behavior demands a large cluster, and we need a large number of independent large clusters to obtain true quenched disorder averages. While the diagonalization of a large number of large matrices is usually very time consuming and inefficient, the Arnoldi-Saad algorithm affords a valuable reduction in the size of the matrices to diagonalize without losing the required information.

It is interesting to note that the region of the spectrum most accurately obtained by our approach is exactly the region of most interest. In previous studies of the eigenspectrum of the fractal diffusion problem [17], the matrix diagonalized was not $\mathbf{W}$ but rather a matrix constructed from the equation of motion for the analogous scalar elasticity problem [15]. For the latter, the important region of the eigenspectrum is near zero (recall the relation $|\ln \lambda| \sim \omega^2$ where ω is the angular frequency of vibration for the scalar elasticity problem). This is where an accurate determination of the spectrum is most difficult by most methods.

A large amount of CPU time and memory is saved by using the Arnoldi-Saad method, which allows the reduction of the dimension of the original matrix without compromising the needed accuracy of the results. For instance, a 5000×5000 $\mathbf{W}$ matrix was reduced by this method typically to one of size 300×300, and the eigenvalues and eigenvectors obtained were reliable to better than one part in 10^5. This operation required about 560 s of CPU time per cluster on a Kubota Pacific Titan P3 minisupercomputer, or less than 30 s on a CPU of a Cray 2 supercomputer, including the cluster generation itself.

The algorithm was described in the literature [13], but we will sketch it here for completeness. In this algorithm, one starts with an arbitrary normalized vector $\mathbf{u}_1$ of dimension S where $\mathbf{W}$ has the dimension of $S \times S$. Then one chooses the subspace dimension $m \leq S$ which is to be the dimension of the reduced upper Hessenberg matrix $\mathbf{H}$ which will then be diagonalized essentially exactly. The reduced matrix $\mathbf{H}$ is obtained recursively and at the same time as a sequence of normalized basis vectors $\mathbf{u}_i$ $(i = 2, ..., m)$ in the following way.

First, the element H_{11} is obtained as $\mathbf{u}_1^T \mathbf{W} \mathbf{u}_1$. Second, the product $\mathbf{v}_2 \equiv H_{21}\mathbf{u}_2$ is calculated as $\mathbf{v}_2 = \mathbf{W}\mathbf{u}_1 - H_{11}\mathbf{u}_1$. We then choose $H_{21} = \|\mathbf{v}_2\|$ to satisfy the normalization requirement $\|\mathbf{u}_2\|^2 = 1$. At the next iteration, we first obtain H_{12} and H_{22} as $\mathbf{u}_1^T \mathbf{W} \mathbf{u}_2$ and $\mathbf{u}_2^T \mathbf{W} \mathbf{u}_2$, respectively, and then $\mathbf{u}_3$ and H_{32} are obtained similarly to the first iteration. This process continues until all elements of $\mathbf{H}$ and all of the $\mathbf{u}_i$ are obtained. In general, we have

$$H_{ij} = \mathbf{u}_i^T \mathbf{W} \mathbf{u}_j, \tag{41}$$

$$H_{j+1,j}\mathbf{u}_{j+1} = \mathbf{W}\mathbf{u}_j - \sum_{i=1}^{j} H_{ij}\mathbf{u}_i, \tag{42}$$

where $\mathbf{u}_i$ $(i = 1, 2, ..., m)$ form an orthonormal set.

This procedure ensures [16] that the eigenvalues of $\mathbf{H}$ are approximate eigenvalues of the original matrix $\mathbf{W}$ and that, if $\mathbf{y}$ is the eigenvector of $\mathbf{H}$ with the eigenvalue λ, then the vector $\mathbf{z}$ defined by its components $z_j \equiv \sum_{i=1}^{m} [u_i]_j y_i$ satisfies the orthogonality

$$(\mathbf{W} - \lambda \mathbf{I})\mathbf{z} \cdot \mathbf{u}_i = 0, \quad i = 1, 2, ..., m. \tag{43}$$

This means that $\mathbf{z}$ is an approximate eigenvector of $\mathbf{W}$ to within the subspace spanned by the $\mathbf{u}_i$'s with the approximate eigenvalue λ.

The approximation is better the larger m is, and also the outer part of the spectrum yields better accuracy [16]. In practice, the eigenvalues pile up at very high density near the outer edge of the spectrum (for p_c), which requires $\mathbf{W}^N$ with a large N (typically greater than 100) to be used in place of $\mathbf{W}$ to separate the eigenvalues. The accuracy of the eigenvalues and eigenvectors can be checked by a number of criteria including one which uses the comparisons between the results obtained by using different dimensions m for the submatrix $\mathbf{H}$, and also by using different N.

VI. NUMERICAL RESULTS

In this section, we summarize the numerical results for the density of states per site $n(\lambda)$, the function $\pi(\lambda)$, and the scaling of the subdominant eigenvalue $\ln\lambda_2$. The calculations have been performed on the triangular, square, and simple cubic lattices as described below.

A. Density of eigenvalues $n(\lambda)$

The density of eigenvalues $n(\lambda)$ has been calculated by accumulating the eigenvalues in logarithmic bins over a large number of independent cluster realizations and then

TABLE I. Number of clusters and other parameters used in the disorder averaging. Size given for the periodic case refers to the grid size.

Lattice	Boundary	Ant	p	Size	Number	Figure
square	nonperiodic	blind	0.593	400	5000	4
			0.593	800	250	4
			0.593	5000	900	4,5,8
	periodic	blind	0.593	100×100	400	5
		myopic	0.593	100×100	250	5,8
		blind	0.75	100×100	250	7,9
			0.9	100×100	200	7,9
simple cubic	nonperiodic	blind	0.312	400	250	4
			0.312	800	300	4
			0.312	5000	500[a]	4,6,8
	periodic	blind	0.312	30^3	449	6
		myopic	0.312	30^3	500[b]	6,8
		blind	0.5	30^3	100	7,9

[a]For Fig. 4, a subset of 449 clusters was used.
[b]For Fig. 8, a subset of 200 clusters was used.

dividing by the number of clusters, the bin width, and the cluster size. The number of independent cluster realizations over which the quenched average is performed for the different cases is tabulated in Table I.

In Fig. 4, $n(\lambda)$ at p_c is plotted against $|\ln\lambda|$ for the blind ant on nonperiodic clusters in $d = 2$ and 3. It is clear from the figure that the data for different cluster sizes collapse into a single curve for both $d = 2$ and 3, showing that finite size effects for $n(\lambda)$ are not important. Note in this and subsequent figures that symbol sizes chosen are larger than the statistical fluctuation.

In order to evaluate the exponent d_s in $d = 2$, a log-log plot is produced for $n(\lambda)$ as a function of $|\ln\lambda|$ in Fig. 5 for the blind and myopic ants on the square lattice. As seen clearly, the data for the blind ant on the periodic and nonperiodic clusters collapse within the statistical errors on the same line of slope -0.35 ± 0.01, showing that boundary conditions do not affect the exponent d_s. The data for the myopic ant on the periodic cluster, on the other hand, yield a least squares fitted line of a slightly larger slope -0.37 ± 0.01. We believe that the small difference in the slopes between the blind and myopic ants is a reflection of the inexact Laplace relationship between $n(\lambda)$ and $P(t)$ for the case of the myopic ant. The blind and myopic ants on a triangular lattice also had a similar slope but they are not shown in the figure to avoid overcrowding.

The exponent d_s for $d = 3$ has similarly been extracted on the simple cubic lattice as shown in Fig. 6. The least square fitted lines for the blind ant on the periodic and nonperiodic lattices have the same slope of -0.35 ± 0.01 within the statistical error, again showing the irrelevance of the boundary conditions for the value of d_s. Here, however, $n(\lambda)$ normalized by the average cluster size for the periodic case does not seem to have the same amplitude as the nonperiodic case. The myopic ant on the simple cubic periodic lattice gave a slightly larger slope of -0.37 ± 0.01, similarly to the case of $d = 2$.

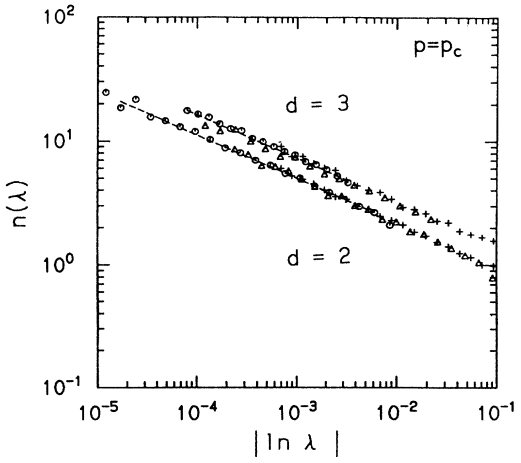

FIG. 4. Density of eigenvalues $n(\lambda)$ normalized by the cluster size for the blind ant on nonperiodic clusters on square and simple cubic lattices. The upper curve corresponds to $d = 3$ and the lower one to $d = 2$. The symbols +, △, and ○ correspond to the cluster sizes 400, 800, and 5000, respectively.

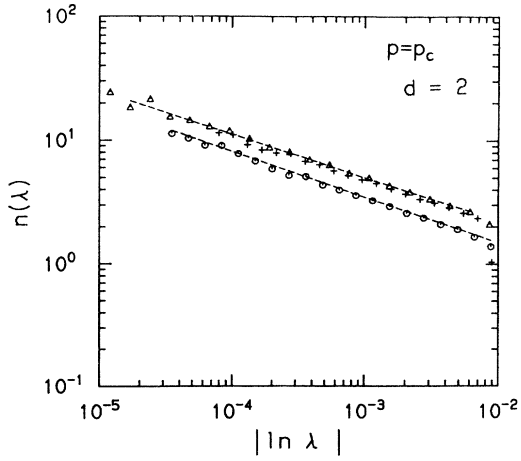

FIG. 5. Log-log plot of $n(\lambda)$ against $|\ln\lambda|$ in $d = 2$ at $p = 0.593 \approx p_c$. The symbols △ and + correspond to the blind ant on a a periodic and nonperiodic square lattices and the symbol ○ corresponds to the myopic ant on a periodic square lattice.

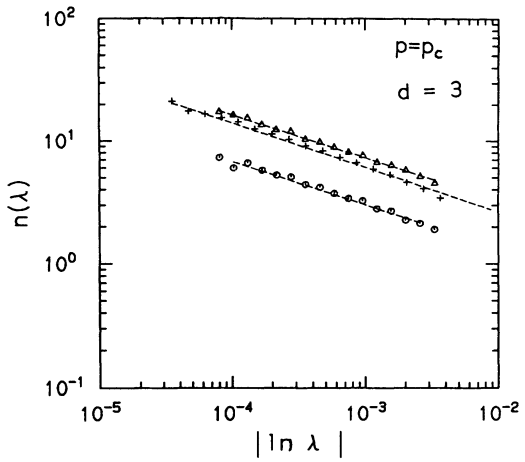

FIG. 6. Log-log plot of $n(\lambda)$ against $|\ln\lambda|$ in $d = 3$ at $p = 0.312 \approx p_c$. The symbols $\triangle$ and $+$ correspond to the blind ant on periodic and nonperiodic simple cubic lattices and the symbol $\circ$ corresponds to the myopic ant on a periodic simple cubic lattice.

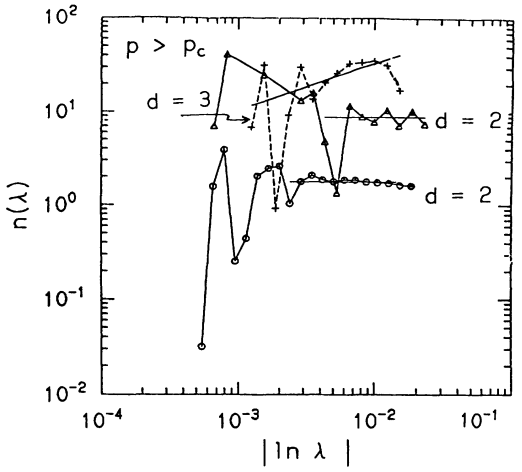

FIG. 7. Log-log plot of $n(\lambda)$ against $|\ln\lambda|$ in $d = 2$ and 3 for $p > p_c$. The symbols $\circ$ and $\triangle$ stand for the blind ant on the periodic square lattice at $p = 0.75$ and $p = 0.9$, respectively, and the symbol $+$ stands for the blind ant on the periodic simple cubic lattice at $p = 0.5$. The lines of slopes zero and $1/2$ are drawn to guide the eye.

The details of the extracted exponent d_s estimates along with the values of the exponent obtained from a standard reference [7] are given in Table II. When these results are compared, we see that they are consistent within the respective errors.

In Fig. 7, a log-log plot of $n(\lambda)$ against $\ln\lambda$ for $p > p_c$ is shown for both $d = 2$ and $d = 3$. In this case, the substrate becomes more ordered and the $n(\lambda)$ is expected to scale as $|\ln\lambda|^{d/2-1}$, where d is the Euclidean dimension of the substrate. Our data show a spiky structure (*not* statistical fluctuations) due to the discrete nature of the eigenvalues. In these figures, lines of expected slope (zero for $d = 2$ and $1/2$ for $d = 3$) are drawn to guide the eye. As is evident from Fig. 7, the data for $d = 3$ have a larger slope than for $d = 2$, as expected.

B. Asymptotic behavior of $\pi(\lambda)$

As discussed earlier, the function $\pi(\lambda)$ at p_c is expected to follow the power law $\pi(\lambda) \sim |\ln\lambda|^{1-2/d_w}$, where d_w is the walk dimension. This exponent is thus extracted from the slope of the log-log plot of $\pi(\lambda)$ versus $|\ln\lambda|$ as shown in Fig. 8. Plotted in this figure are the results from the blind ant for nonperiodic clusters on the square and simple cubic lattices and those from the myopic ant for periodic clusters on the same two lattices (for λ near 1 and *not* -1, as discussed in Sec. III). Some data points toward both ends of $|\ln\lambda|$ were not included where they correspond to partially filled bins (i.e., only some cluster realizations have eigenvalues falling in these bins).

The estimated value of $1-2/d_w$ for $d = 2$ is 0.30 ± 0.01 for the myopic ant on the periodic square grid and 0.27 ± 0.01 in the case of the blind ant on the nonperiodic square grid. (The estimates for the periodic lattice are actually identical for both the blind and myopic ants.) In $d = 3$ the slope of the least squares fit was found to be 0.46 ± 0.02 for the myopic ant on the nonperiodic simple cubic grid and 0.43 ± 0.01 for the blind ant for the nonperiodic case. The exponents calculated from the slopes for the data for the periodic lattice agree very well with the

TABLE II. Estimates of $d_s/2-1$ from the density of eigenvalues $n(\lambda)$.

d	This work	Using d_s from [7]	$d/2-1$ (for $p > p_c$)
2	-0.35 ± 0.01	-0.347 ± 0.013	0
3	-0.35 ± 0.01	-0.336 ± 0.003	1/2

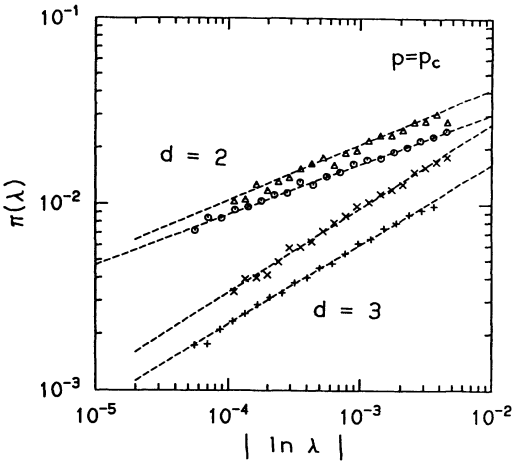

FIG. 8. Log-log plot of $\pi(\lambda)$ against $|\ln\lambda|$ in $d = 2$ and 3 at $p = p_c$. The symbols $\triangle$ and $\circ$ stand for the myopic ant on the periodic square lattice and the blind ant on the nonperiodic square lattice, respectively, and the symbols $\times$ and $+$ correspond to the myopic ant on the periodic simple cubic lattice and the blind ant on the nonperiodic simple cubic lattice, respectively.

previously available ones from Ref. [7] within the respective errors. Although our slope estimates themselves are substantially different between the periodic and nonperiodic clusters, the corresponding exponents d_w calculated from these slopes do not differ quite as much. While the remaining deviations are still larger than the statistical errors and thus a source of concern, we believe that the periodic lattice results are inherently more trustworthy and the nonperiodic lattice results are somehow reflecting the more severe boundary effects and/or the effects of the cluster geometry imposed by arbitrarily stopping the cluster growing algorithm at a predetermined size. We do not, however, understand why this effect seems to be much more prominent for $\pi(\lambda)$ than for $n(\lambda)$.

In Fig. 9 a log-log plot of $\pi(\lambda)$ against $|\ln\lambda|$ for $p > p_c$ is presented. For $p > p_c$, the function $\pi(\lambda)$ is expected to behave like $|\ln\lambda|^{d/2}$ as $\lambda \to 1$. Again in this case we find some structure in the data, and lines of slope 1 and 1.5 are drawn in the figure to guide the eye. For $d = 2$, the data were collected at $p = 0.75$ and $p = 0.9$, and for $d = 3$, the data were collected for $p = 0.5$. The number of clusters over which the average was taken is the same as the corresponding data for $n(\lambda)$. Again it is evident from the figure that the slope of $\pi(\lambda)$ in the case of $d = 3$ is larger than in $d = 2$, as expected. The summary of all these results is given in Table III.

TABLE III. Estimates of $1 - 2/d_w$ from $\pi(\lambda)$.

d	This work	Using d_w from [7]	$d/2$ (for $p > p_c$)
2	0.30 ± 0.01	0.30 ± 0.01	1
3	0.46 ± 0.01	0.46 ± 0.03	3/2

C. Subdominant eigenvalue λ_2

The values of the maximum eigenvalue below 1, λ_2, in two and three dimensions are plotted in Fig. 10 against the cluster size. The details of the cluster sizes along with the number of independent cluster realizations over which the average was taken are tabulated in Table IV. (We may note that the number of clusters sampled for $p > p_c$ in $d = 2$ was in fact far more than necessary.) The accuracy in the numerical evaluation of λ_2 was better than one part in 10^6 in all cases.

As discussed above, the subdominant eigenvalue $\ln\lambda$ scales with the size of the cluster, S, as $|\ln\lambda_2| \sim S^{-d_w/d_f}$ at $p = p_c$. We have extracted this exponent d_w/d_f from the slope of the log-log plot of $|\ln\lambda_2|$ versus S as shown in Fig. 10. The straight lines drawn are linear least square fits and all of them have a correlation coefficient of greater than 0.9999.

In $d = 2$ we have obtained a slope magnitude of 1.546 ± 0.019 for the myopic ant on the triangular lattice and a slope of 1.529 ± 0.004 for the blind ant on the square lattice. In comparison, using the previously available best estimate of $d_s = 1.30 \pm 0.002$ as given in Ref. [7], and assuming the scaling relation $d_s = 2d_f/d_w$, we would get the corresponding value of $d_w/d_f = 1.538 \pm 0.024$. Thus we see that our estimate computed from the finite size scaling of the subdominant eigenvalues is in excellent agreement with the direct simulation result (and the scaling relation used).

In $d = 3$ the value of the slope magnitude obtained is 1.508 ± 0.007. Again using the value of $d_s = 1.328 \pm 0.006$ from Ref. [7] and the relation $d_s = 2d_f/d_w$, the simulation estimate of this quantity would come out to be 1.506 ± 0.007, again in excellent agreement with our analysis. The summary of these results is given in Table V.

In order to check the finite size scaling relation for $|\ln\lambda_2|$ for p close to but greater than p_c, in Fig. 11 we plot $|\ln\lambda_2|S^{2/d_s}$ against $(p - p_c)S^{\sigma}$ for three different values of $p > p_c$ in $d = 2$ and 3, respectively, where $\sigma = 1/(d_f\nu)$.

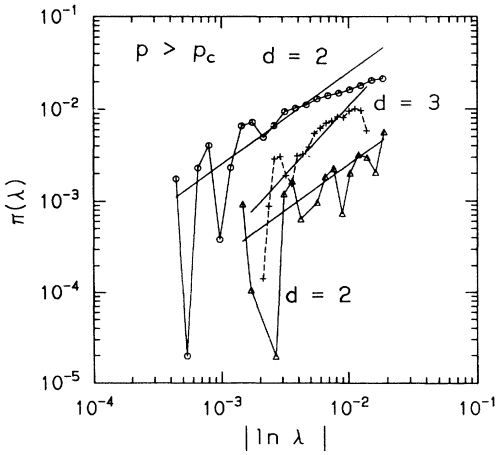

FIG. 9. Log-log plot of $\pi(\lambda)$ against $|\ln\lambda|$ in $d = 2$ and 3 for $p > p_c$. The symbols ○ and △ stand for the blind ant on the periodic square lattice at $p = 0.75$ and $p = 0.9$, respectively. The symbol + stands for the blind ant on the periodic simple cubic lattice at $p = 0.5$.

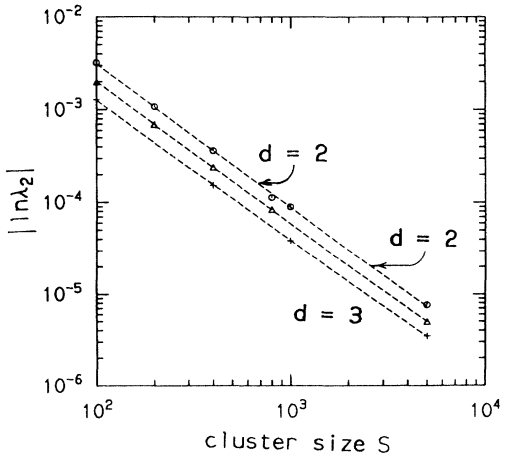

FIG. 10. Log-log plot of $|\ln\lambda_2|$ against the size S of the cluster. The symbol ○ corresponds to the myopic ant on the triangular lattice. The symbols △ and + correspond to the blind ant on the square and simple cubic lattices, respectively.

TABLE IV. Cluster ensembles used in the disorder averaging for λ_2.

Lattice, Ant	p	Size	Number
triangular, myopic; square, blind	0.5 (tr) ; 0.593 (sq)	100	10000
		200	5000
		400	5000
		800	2500
		1000	2500
		5000	1000
square, blind	0.33, 0.34, 0.35	100	10000
		400	10000
		1000	5000
		5000	1000
simple cubic, blind	0.312	100	10000
		400	5000
		1000	2500
		5000	1000
simple cubic, blind	0.64, 0.65, 0.66	100	100
		400	250
		1000	300
		5000	1000

As is evident from the figure, both in $d = 2$ and 3, the data for different values of p collapse onto a single curve, which is the universal scaling function $f(x)$ [where $x = (p - p_c)S^\sigma$], supporting the scaling form given by Eq. (37). The scaling function is numerically fitted to a quadratic curve of the form $ax^2 + bx + c$ as shown by the dashed lines in the figure. The values for the coefficients a, b, and c have been numerically estimated as 2.646, 0.893, and 2.358 from the square lattice data and 0.894, 0.276, and 1.044 from those on the simple cubic lattice, respectively. Even though $f(x)$ is expected to depend only on the dimensionality, in general there will be lattice-dependent *metrical* factors which will affect the values of the coefficients.

The nonzero value of c indicates that $f(x)$ indeed tends to a nonzero constant in the limit $x \to 0$. This is consistent with the scaling relationship for $|\ln \lambda_2|$ at $p = p_c$. Our scaling prediction for the value of the exponent z is 1.21 for $d = 2$ and 1.81 for $d = 3$, respectively, from Eq. (38). The value of z was not estimated numerically since it is valid only in the asymptotic limit $x \to \infty$, thus needing the calculation of λ_2 for cluster sizes larger than available due to computational limitations.

VII. SUMMARY

In summary, we used the Arnoldi-Saad algorithm [16] to approximately diagonalize the hopping transition matrix and successfully extracted the dynamical exponents d_w and d_s at the critical value of p for the percolation cluster. We found that, for $p > p_c$, the eigenvalue spectrum reflects the discrete, local lattice structure more clearly, and mainly because of this there is a spiky nonstatistical structure in the density of states. Despite the numerical difficulty caused by this, we clearly observe the crossover between the fracton regime (anomalous diffusion) and the phonon regime (Euclidean diffusion with a long-time tail).

We have also proposed a scaling relation for the subdominant eigenvalue λ_2 and shown that it can be used as the most computationally efficient method to extract the critical exponent combination d_w/d_f (which is equal to $2/d_s$ for percolation). The computational efficiency is due to the fact that only the largest eigenvalue (below 1)

TABLE V. Estimates of d_w/d_f from $\ln \lambda_2$.

d	Ant type	This work	Using $2/d_s$ from [7]
2	myopic	1.546 ± 0.019	1.538 ± 0.024
2	blind	1.529 ± 0.004	1.538 ± 0.024
3	blind	1.508 ± 0.007	1.506 ± 0.007

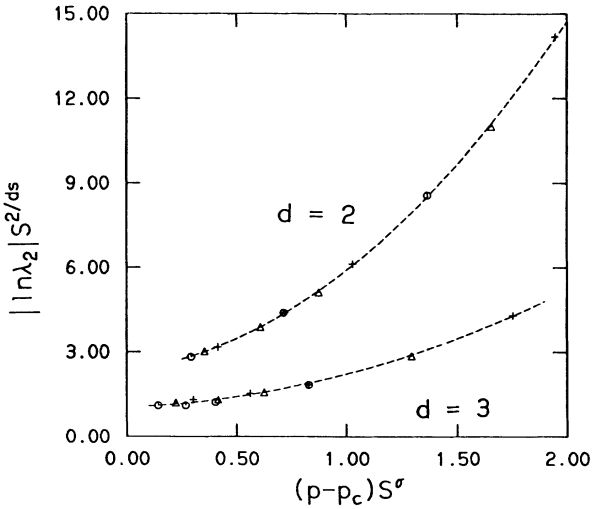

FIG. 11. Finite size scaling of $|\ln \lambda_2|$ with respect to the size of the cluster and $(p - p_c)$. Quadratic fits for the universal scaling functions $f(x)$ are shown in dashed lines, where $x = (p - p_c)S^\sigma$ and the upper curve corresponds to $d = 2$, the lower to $d = 3$.

has to be evaluated.

The method of eigenspectrum analysis presented here reduces the study of diffusion in complex, random media to that of certain kinds of large, random matrices. It is important to note, however, that the randomness treated here is the direct result of the quenched disorder in the environment and thus the random matrix has a specific sparse structure and correlation among its nonzero elements, reflecting the geometry of a particular connected cluster. The correlation among the matrix elements in this sense unfortunately makes the mathematical analysis of these random matrices much more difficult than those with independently distributed elements, which most studies of the so-called random matrix theory [20] deal with. This is part of the reason why most of our results have been obtained by the numerical analysis of these matrices.

This type of numerical analysis can be carried out with very high precision in a systematic way taking the best advantage of modern computing equipment (with vector and parallel processing). In fact, this approach was recently applied by us to a number of problems including the *scalar* elasticity of *loop-enhanced* structures [18] and a study of the breakdown of the scaling relation $d_s = 2d_f/d_w$ for treelike structures [19]. Further applications contemplated include the problem of diffusion in an external velocity field, a possible model of Brownian transport in the presence of macroscopic convection.

ACKNOWLEDGMENTS

We appreciate fruitful discussions with J. W. Halley, A. Giacometti, Hans J. Herrmann, R. Muralidhar, and especially D. J. Jacobs. This work was supported in part by a grant from ONR and we are grateful for the generous use of computer time at the Supercomputer Center of the Naval Oceanographic Office.

APPENDIX A: BOUNDS ON THE EIGENVALUES OF A MARKOV MATRIX

The well-known property that the eigenvalues of a Markov matrix $\mathbf{W}$ satisfy $|\lambda| \leq 1$ is proven here for completeness. Let u_j be the left eigenvector of $\mathbf{W}$ corresponding to the eigenvalue λ; then

$$\sum_j W_{ij} u_j = \lambda u_i. \tag{A1}$$

Taking the modulus of the above equation, we get

$$\left| \sum_j W_{ij} u_j \right| = |\lambda| |u_i|, \tag{A2}$$

$$\sum_j W_{ij} |u_j| \geq |\lambda| |u_i|. \tag{A3}$$

Now summing over the index i in the above equation, we get

$$\sum_j |u_j| \sum_i W_{ij} \geq |\lambda| \sum_i |u_i|, \tag{A4}$$

$$\sum_j |u_j| \geq |\lambda| \sum_i |u_i|. \tag{A5}$$

We have made use of the second property of the Markov matrix $\sum_i W_{ij} = 1$. This completes the proof.

APPENDIX B: SYMMETRIZATION OF A MARKOV MATRIX WITH DETAILED BALANCE

A Markov matrix $\mathbf{W}$ satisfying the detailed balance condition can be symmetrized as follows. The detailed balance condition for $\mathbf{W}$ is given by

$$W_{ij} \rho_j^e = W_{ji} \rho_i^e, \tag{B1}$$

Taking the square root of the above equation we get

$$(W_{ij})^{1/2} (\rho_j^e)^{1/2} = (W_{ji})^{1/2} (\rho_i^e)^{1/2}. \tag{B2}$$

Now, let the matrix $\mathbf{A}$ be diagonal with the ith diagonal element equal to $(\rho_i^e)^{1/2}$. Then its inverse $\mathbf{A}^{-1}$ is also diagonal with its jth diagonal element equal to $(\rho_j^e)^{-1/2}$. We will show that the matrix $\mathbf{A}^{-1}\mathbf{W}\mathbf{A}$ is symmetric. Let us consider the ijth element $(\rho_i^e)^{-1/2} W_{ij} (\rho_j^e)^{1/2}$ of this matrix:

$$\begin{aligned}(\rho_i^e)^{-1/2} W_{ij} (\rho_j^e)^{1/2} &= (\rho_i^e)^{-1/2} (W_{ij})^{1/2} (W_{ij})^{1/2} (\rho_j^e)^{1/2} \\ &= (\rho_j^e)^{-1/2} (W_{ji})^{1/2} (W_{ji} \rho_i^e)^{1/2} \\ &= (\rho_j^e)^{-1/2} W_{ji} (\rho_i^e)^{1/2},\end{aligned} \tag{B3}$$

which is just the jith element. This completes the proof.

APPENDIX C: EXPANSION COEFFICIENTS a_λ FOR PERIODIC BOUNDARIES

We show in this section how the calculation of the expansion coefficients a_λ which appear in the function $\pi(\lambda)$ can be obtained from the *velocity* vectors. From Eqs. (21)–(24), we have

$$a_\lambda = \sum_s v_\lambda(s) \mathbf{r}(s) \cdot \sum_{s_0} u_\lambda(s_0) \rho(s_0) \mathbf{r}(s_0), \tag{C1}$$

where $\mathbf{u}_\lambda^T$ and $\mathbf{v}_\lambda$ are normalized left and right eigenvectors of $\mathbf{W}$ for the eigenvalue λ, ρ is the initial probability distribution, and the dot product refers to the coordinate space as before.

Replacing the coordinate vectors $\mathbf{r}(s)$ by the velocity vectors $[\mathbf{r}(s) - \mathbf{r}(s_i)]$, where the sites s_i are the nearest neighbors of the site s, the first of the two factors in the above equation becomes

$$\begin{aligned}\sum_s v_\lambda(s) \mathbf{r}(s) = \sum_s v_\lambda(s) \frac{1}{z(s)} \sum_{i=1}^{z(s)} [\mathbf{r}(s) - \mathbf{r}(s_i)] \\ + \sum_s v_\lambda(s) \frac{1}{z(s)} \sum_{i=1}^{z(s)} \mathbf{r}(s_i).\end{aligned} \tag{C2}$$

Here $z(s)$ is the number of occupied neighbors of the site s in the case of the myopic ant. For the blind ant, $z(s)$ stands for the lattice coordination number and, if the ith neighbor is not a cluster site, then $s_i \equiv s$ is understood.

The second term on the right can be simplified by exchanging the summations over s and s_i:

$$\sum_s v_\lambda(s)\frac{1}{z(s)}\sum_{i=1}^{z(s)}\mathbf{r}(s_i) = \sum_{s'}\mathbf{r}(s')\sum_{i=1}^{z(s')}\frac{1}{z(s_i')}v_\lambda(s_i') = \sum_{s'}\mathbf{r}(s')\lambda v_\lambda(s') = \lambda\sum_{s'}\mathbf{r}(s')v_\lambda(s'), \tag{C3}$$

where we used the relation

$$\sum_{i=1}^{z(s')}\frac{1}{z(s_i')}v_\lambda(s_i') = \sum_{s''}W(s',s'')v_\lambda(s''). \tag{C4}$$

Therefore we get

$$\sum_s v_\lambda(s)\mathbf{r}(s) = \frac{1}{(1-\lambda)}\sum_s v_\lambda(s)\frac{1}{z(s)}\sum_{i=1}^{z(s)}[\mathbf{r}(s)-\mathbf{r}(s_i)]. \tag{C5}$$

Similarly the second factor in Eq. (C1) is

$$\sum_s u_\lambda(s)\mathbf{r}(s)\rho(s) = \frac{1}{(1-\lambda)}\sum_s u_\lambda(s)\rho(s)\frac{1}{z(s)} \times\sum_{i=1}^{z(s)}[\mathbf{r}(\mathbf{s})-\mathbf{r}(s_i)]. \tag{C6}$$

Once in this form, the absolute coordinates are not required; rather, only the nearest neighbor *velocities* are. In the calculation of the expansion coefficients a_λ, then, we only need to keep track of the velocity vectors. This is necessary in the case of the periodic boundary conditions; although it is not necessary in the nonperiodic case, it can also be applied there.

[1] *Random walks and Their Applications in the Physical and Biological Sciences*, edited by Michael F. Shlesinger and Bruce J. West, AIP Conf. Proc. No. 109 (AIP, New York, 1984).

[2] J. P. Straley, in *Electrical Transport and Optical Properties of Inhomogeneous Media*, edited by J. C. Garland and D. B. Tanner, AIP Conf. Proc. No. 40 (AIP, New York, 1978), and references therein.

[3] P. G. de Gennes, *Scaling Concepts in Polymer Physics* (Cornell University, Ithaca, 1979), and references therein.

[4] J. des Cloiseaux and G. Jannik, *Polymers in Solution: Their Modelling and Structure* (Oxford, New York, 1990), and references therein.

[5] D. Stauffer and A. Aharony, *Introduction to Percolation Theory* (Taylor and Francis, London, 1992).

[6] B. Mandelbrot, *Fractal Geometry of Nature* (Freeman, San Francisco, 1982).

[7] S. Havlin and D. Ben-Avraham, Adv. Phys. **36**, 695 (1987), and references therein.

[8] N. G. van Kampen, *Stochastic Processes in Physics and Chemistry* (North-Holland, Amsterdam, 1981).

[9] Y. Gefen, A. Aharony, and S. Alexander, Phys. Rev. Lett. **50**, 77 (1983).

[10] B. J. Alder and W. E. Alley, J. Stat. Phys. **19**, 341 (1978); Physica A **121**, 523 (1983).

[11] M. H. Ernst and A. Weyland, Phys. Lett. **34A**, 39 (1971).

[12] H. Nakanishi, S. Mukherjee, and N. H. Fuchs, Phys. Rev. E **47**, R1463 (1993).

[13] N. H. Fuchs and H. Nakanishi, Phys. Rev. A **43**, 1721 (1991).

[14] D. J. Jacobs and H. Nakanishi, Phys. Rev. A **41**, 706 (1990).

[15] S. Alexander and R. Orbach, J. Phys. (Paris) Lett. **43**, 625 (1982).

[16] Y. Saad, Linear Algebra Appl. **34**, 269 (1980); see also W. E. Arnoldi, Q. Appl. Math. **9**, 17 (1951).

[17] K. Yakubo and T. Nakayama, Phys. Rev. B **40**, 517 (1989).

[18] H. Nakanishi, Physica A **196**, 33 (1993).

[19] H. Nakanishi and H. J. Herrmann, J. Phys. A **26**, 4513 (1993).

[20] See, e.g., M. L. Mehta, *Random Matrices* (Academic Press, San Diego, 1991).